NASA Technical Memorandum 78579

Vortex Simulation of Three-Dimensional, Spotlike Disturbances in a Laminar Boundary Layer

A. Leonard

May 1979

National Aeronautics and
Space Administration

NASA Technical Memorandum 78579

Vortex Simulation of Three-Dimensional, Spotlike Disturbances in a Laminar Boundary Layer

A. Leonard, Ames Research Center Moffett Field, California

NASA
National Aeronautics and
Space Administration

Ames Research Center
Moffett Field, California 94035

VORTEX SIMULATION OF THREE-DIMENSIONAL, SPOTLIKE DISTURBANCES IN A LAMINAR BOUNDARY LAYER *

A. Leonard

Ames Research Center, NASA, Moffett Field, California 94035 U.S.A.

ABSTRACT

The growth of a turbulent spot in a laminar boundary layer, as the spot evolves from a localized disturbance in the layer, is simulated numerically using a three-dimensional vortex filament description of the vorticity field. The filaments are marked with a sequence of node points which are tracked in a Lagrangian reference frame. Velocity computation is done by Biot-Savart integration. Although some discrepancies with experiment appear to exist in the near wall region, the gross properties of the spot, including the velocities of the leading and trailing edges and the velocity perturbations away from the wall, are in good agreement with experiment.

INTRODUCTION

Studies of the turbulent spot in a laminar boundary layer date back to the theoretical and experimental work of Emmons (1) and Mitchner (2), who were concerned with the role of spots in the transition process. Such spots are now recognized as interesting flow phenomena in their own right and, in addition, spots or spotlike objects have been suggested as the coherent flow structure responsible for much of the turbulent transport in a fully developed turbulent boundary layer (3,4). Recent experiments by Wygnanski, et al. (5) and Cantwell, et al. (6) confirmed earlier observations of Schubauer and Klebanoff (7) and provided much new information on the structure of turbulent spots. In particular, entrainment rates in the plane of symmetry and the mean flow field within the spot were obtained by ensemble averaging over a large number of spots. In another recent experiment, Gaster and Grant (8) studied the evolution of a wave packet in a laminar boundary layer produced by a localized perturbation at the wall boundary. The amplitude of the perturbation was very small so that the linear development of the resultant disturbance could be observed for some time after its initiation. Indeed, model calculations by Gaster (9) based on linear theory agree well with the experimental measurements of Gaster and Grant (8) during the early stages, but some qualitative differences were noted in the later stages of growth, presumably due to nonlinear mechanisms.

Despite these significant advances in our understanding of turbulent spots, a number of questions remain, such as the interaction of two or more spots, the formation of sublayer streaks, the three-dimensional vorticity field within the spot, the nonlinear mechanics of growth, and the birth of new spots.

In this paper, the growth of a turbulent spot in a laminar boundary layer, as the spot evolves from a localized disturbance in the layer, is simulated numerically using a vortex filament description of the vorticity field. The attempt is to provide additional insight into the structure and growth of a turbulent spot. In many respects, the method employed (10,11) is an extension to three dimensions of the two-dimensional vortex method (12,13) and is done in the spirit of the large-eddy simulation technique (14) in which small-scale turbulence is not simulated directly but is modeled. In an earlier numerical study Hama (15), motivated by his experimental observations of boundary-layer transition, investigated the motion of a single vortex loop.

Previous three-dimensional numerical simulations of wall-bonded shear flows have included channel flow simulations by Deardorff (16) and Schumann (17) using an artificial law-of-the-wall boundary condition and the recent improved simulation by Moin et al. (18) using the no-slip condition. In addition, transition phenomena have been simulated numerically by Orszag (19) and by Wray et al. (20).

NUMERICAL METHOD

For numerical purposes, a turbulent spot is viewed as a localized region of boundary-layer vorticity that has undergone three-dimensional displacements, strains, and rotations from its original monodirectional laminar state (see Fig. 1). Each tube of vorticity in the boundary layer is decomposed into its straight, unperturbed contribution and into a loop representing its contribution to the perturbed vorticity field, as shown in Fig. 2. The velocity field is decomposed, accordingly, as

$$\underline{u}(\underline{x}) = U(y)\hat{e}_x + \underline{u}'(\underline{x})$$

where $U(y)$ is the laminar profile and $\underline{u}'$ is given by a sum of Biot-Savart integrations over all the filament curves, C_i, plus their images. The image contributions ensure tangency of the flow at the wall. In this initial study we ignore the generation of vorticity at the wall boundary due to the disturbance, i.e., we use the inviscid boundary condition at the wall. Biot-Savart integration yields an exact representation of the boundary conditions at infinity in all directions.

Each filament is represented by a space curve $\underline{x}_i(\xi,t)$, where ξ is a parameter along the curve; by a circulation Γ_i; and by an effective core radius σ_i, which parameterizes the assumed Gaussian vorticity distribution within the filament. Thus the perturbed vorticity field is given by

$$\underline{\omega}(\underline{x},t) = \sum_i \Gamma_i \oint_{C_i} \exp[-|\underline{x}-\underline{x}_i|^2/\sigma_i^2]/(\sqrt{\pi}\sigma_i)^3 \frac{\partial \underline{x}_i}{\partial \xi}\, d\xi$$

---

*Presented at the Second Symposium on Turbulent Shear Flows, July 2-4, 1979, Imperial College, London, England.

A filament or curve represents a collection of vortex lines so that the filament velocity must be computed as an appropriate average over the filament core. We use the following equation of motion for the space curves:

$$\frac{\partial \underline{x}_i}{\partial t} = -\frac{1}{4\pi}\sum_j \Gamma_j \oint_{C_j} \frac{(\underline{x}_i - \underline{x}_j)\times \frac{\partial \underline{x}_j}{\partial \xi'}\, d\xi'}{[|\underline{x}_i - \underline{x}_j|^2 + \alpha(\sigma_i^2 + \sigma_j^2)]^{3/2}}$$

$$+ \hat{e}_x U(y_i) + \text{image contributions}$$

The equation is seen to be the Biot-Savart induction law for an infinitesimal filament but corrected in the near field for finite core size. Using $\alpha = 0.2065$ we recover the correct speed of a ring vortex in the limit $\sigma_i \ll$ ring radius.

For numerical purposes, the filaments are marked with a sequence of node points which are tracked in a Lagrangian reference frame. The space curve $\underline{x}_i(\xi,t)$ is assumed piecewise linear, passing through each node point. The spacing between node points is $O(\sigma_i)$ to minimize discretization error. For example, satisfying this constraint yields a computed speed of a ring vortex that is essentially independent of the number of node points.

Discretization in the directions normal to the vorticity vector must also be treated carefully. If the nominal spacing between vortices is so large that adjacent cores do not overlap, the smooth vorticity field that exists in the undisturbed regions near the spot is poorly approximated. Given a number of horizontal layers of vortex filaments, equally spaced in the vertical direction, an optimum core size as well as a set of optimum circulations for each horizontal layer is determined that minimizes the mean square error in the desired vorticity distribution. The result of this procedure is displayed in Fig. 3(a) for the case of eight layers, whereas the effect of choosing a smaller value of core size is shown in Fig. 3(b).

For many incompressible flows in which the vorticity is concentrated in small regions, vortex methods have the conceptual advantage that computational points need only appear in the vorticity-containing regions. In this problem only the region of perturbed vorticity requires points. Thus, in this simulation, points are added automatically in the streamwise and, in some cases, the spanwise direction, as the spot grows. More specifically, the maximum perturbation of $\underline{x}_i$ in the farthest upstream and farthest downstream filaments in each layer is monitored. As soon as that perturbation reaches a critical value (usually 0.004 of the displacement thickness, δ^*) a new, adjacent filament is added. This feature, which helps minimize the number of computational points, is particularly important because $O(N^2)$ operations per time step are required to compute the velocity at each of N vortex node points. For reasonable total run times (1-2 cpu hr), the maximum number of points representing one-half the spot is <2000 on the CDC 7600 and <8000 on the Illiac IV.

The range of computed scales of motion is quite large; e.g., in the streamwise direction the ratio of the largest to the smallest computed scale is ~125 to 1. Nevertheless, this range is not large enough to span those scales found experimentally (see, e.g., aluminum particle photographs in Ref. 6). Thus, the effect of the smaller or subgrid scales on the computed scales must be modeled. The usual procedure used in finite-difference simulations is to use a subgrid viscosity dependent on the local strain rate (14). In this study we simply maintain a constant filament core size. Indeed, this procedure is basically equivalent to using a subgrid viscosity dependent on the local rate of vortex stretching.

RESULTS

Figure 4 displays the computed grid of vortex filaments as the spot develops. All the results given in this paper were obtained on the Illiac IV, although development of the algorithm was done on a CDC 7600. As shown at $t = 0$, the initial perturbation imposed on the boundary layer consists of a localized deformation of the vortex lines in the streamwise direction with a maximum displacement equal to 0.3. The net effect of this deformation is equivalent to adding a ringlike blob of vorticity to the laminar boundary layer, oriented so that the blob is initially moving upward away from the plate. The maximum streamwise velocity perturbation in this initial disturbance is $-0.07\ U_\infty$. Velocities and lengths are normalized so that $U_\infty = 1$ and $\partial U/\partial y|_{wall} = 1$. The unperturbed vorticity profile is that shown in Fig. 3(a) and the corresponding δ^* is 1.21. Eight levels of filaments were used in the y-direction normal to the plate and were spaced 0.2 apart. The same spacing was used in the streamwise (x) direction due to the isotropy of the velocity field induced by each filament. The initial spacing of points along each filament was 0.67. As the simulation proceeded, however, points were automatically redistributed to provide a higher density of points in regions of high curvature. The lifting of vortex lines is evident in the side view of Fig. 4. The stretching of vortex lines and the development of streamwise vorticity is quite evident in the plan view. In the simulation shown in Fig. 4, 2184 points in 104 filaments were used at $t = 0$. At the end of the run of 71 steps ($\Delta t = 0.3$, first-order Euler explicit time differencing), there were 12,222 points in 582 filaments representing the spot. The spot was assumed to be symmetric with respect to the $z = 0$ plane. Therefore, the number of computational points requiring nodal velocities was only approximately half the total number representing the disturbance.

In Fig. 5, a time sequence of contour plots is shown for the perturbed streamwise velocity in the plane of symmetry. The plots are dominated by a growing patch of streamwise velocity deficit with a peak of $-0.37\ U_\infty$ at the final time, $t = 21$. Small regions of positive perturbation are evident near the wall in the later stages. Corresponding plots of vertical velocity and perturbed spanwise vorticity are shown in Figs. 6 and 7, respectively. As shown, the vertical velocities are predominately positive. The vorticity plot shows an elongated region of negative vorticity riding on a similar region of positive vorticity.

To compare with experiment, profiles of the spot boundary were determined from plots similar to those in Fig. 5 according to the criterion of Ref. 5: 2% deviation of the streamwise velocity from its free-stream value. Shown in Fig. 8 are trajectories of the leading and trailing edges measured in the plane of symmetry at $y = 0.6$, 0.9, and 1.2. (These y values have undisturbed laminar velocities of $0.55\ U_\infty$, $0.75\ U_\infty$, and $0.89\ U_\infty$, respectively.) The trajectories for $y = 1.2$ yield leading- and trailing-edge velocities of $0.88\ U_\infty$ and $0.48\ U_\infty$, respectively. These values compare well with those of Wygnanski et al. (5), who found $U_{LE} = 0.89\ U_\infty$ and $U_{TE} = 0.50\ U_\infty$, and with those of Schubauer and Klebanoff (7), who reported $U_{LE} = 0.88\ U_\infty$ and $U_{TE} = 0.50\ U_\infty$. Trailing-edge velocities, however, show a significant variation with y. The plot also reveals the virtual origin (x_o, t_o) of the spot.

Velocity histories at fixed points are shown in Figs. 9 and 10. The u-velocity records away from the wall show the characteristic dip and recovery in agreement with the measurements of Refs. 5 and 6 based on ensemble means over large numbers of spots. The simulated u-velocities in the plane of symmetry near the wall show no indication of the high-speed rise which is observed experimentally. The normal velocity record shown in Fig. 10 has an initial dip followed by a rise to positive values in agreement with the ensemble-averaged results of Ref. 5.

Streamwise velocity perturbations in three horizontal planes at $t = 18$ are shown in Fig. 11. Although the velocity histories taken in the plane of symmetry (Fig. 9) showed no evidence of high-speed fluid near the wall, the contour plot for $y = 0.3$ shows extensive regions of positive perturbation away from the plane of symmetry.

CONCLUSIONS

The numerical simulation of a spotlike disturbance in a laminar boundary layer using vortex filaments has provided insight into the development of the three-dimensional vorticity and velocity fields within the spot. Gross properties of the spot away from the wall, including the velocities of the leading and trailing edges and the velocity perturbations, are in good agreement with experiment.

Discrepancies with experiment appear to exist in the near wall region, especially at the trailing edge. This suggests that future simulations should include the effect of vorticity production at the wall and an improved representation of viscous dissipation. Another source of disagreement may be the relatively short history of the computed spot. Experimental results (5-7) are based on spots that have traveled several hundred δ^* whereas the computed spot has traveled about 20 δ^*. Another possibility is that the experimental data were obtained from ensemble averaging over a large number of spots, a procedure that possibly filters out important coherent motions on the scale of several δ^* or more in addition to unwanted "noise."

ACKNOWLEDGMENT

The author thanks Dr. R. S. Rogallo for reprogramming the original CDC 7600 code for use on Illiac and for many helpful suggestions.

REFERENCES

1 Emmons, H. W., "The Laminar-Turbulent Transition in a Boundary Layer, Part I," Journal of the Aeronautical Sciences, Vol. 18, No. 7, July 1951, pp. 490-498.

2 Mitchner, M., "Propagation of Turbulence from an Instantaneous Point Disturbance," Journal of the Aeronautical Sciences, Vol. 21, No. 5, May 1954, pp. 350-351.

3 Coles, D. and Barker, S. J., "Some Remarks on a Synthetic Turbulent Boundary Layer," Turbulent Mixing in Nonreactive and Reactive Flows, Plenum Press, 1975, pp. 285-292.

4 Offen, G. R. and Kline, S. J., "Combined Dye-Streak and Hydrogen-Bubble Visual Observations of a Turbulent Boundary Layer," Journal of Fluid Mechanics, Vol. 62, Part 2, Jan. 1974, pp. 223-239.

5 Wygnanski, I., Sokolov, M., and Friedman, D., "On a Turbulent 'Spot' in a Laminar Boundary Layer," Journal of Fluid Mechanics, Vol. 78, Part 4, Dec. 1976, pp. 785-819.

6 Cantwell, B., Coles, D., and Dimotakis, P., "Structure and Entrainment in the Plane of Symmetry of a Turbulent Spot," Journal of Fluid Mechanics, Vol. 87, Part 4, Aug. 1978, pp. 641-672.

7 Schubauer, G. B. and Klebanoff, P. S., "Contributions on the Mechanics of Boundary-Layer Transitions," NASA TN 3489, Sept. 1955.

8 Gaster, M. and Grant, I., "An Experimental Investigation of the Formation and Development of a Wave Pocket in a Laminar Boundary Layer," Proceedings of the Royal Society of London, Vol. A347, Dec. 1975, pp. 253-269.

9 Gaster, M., "A Theoretical Model of a Wave Pocket in the Boundary Layer on a Flat Plate," Proceedings of the Royal Society of London, Vol. A347, Dec. 1975, pp. 271-289.

10 Leonard, A., "Numerical Simulation of Interacting, Three-Dimensional Vortex Filaments," Proceedings of the Fourth International Conference on Numerical Methods in Fluid Dynamics, Springer-Verlag, New York, 1975, pp. 245-250.

11 Leonard, A., "Simulation of Three-Dimensional Separated Flows with Vortex Filaments," Proceedings of the Fifth International Conference on Numerical Methods in Fluid Dynamics, Springer-Verlag, New York, 1976, pp. 280-284.

12 Chorin, A. J., "Numerical Study of Slightly Viscous Flow," Journal of Fluid Mechanics, Vol. 57, Part 4, Mar. 1973, pp. 785-796.

13 Ashurst, W. T., "Numerical Simulation of Turbulent Mixing Layers via Vortex Dynamics," Proceedings of the Symposium on Turbulent Shear Flows, Vol. I, Pennsylvania State University, 1977, pp. 11.43-11.50.

14 Ferziger, J. H., "Large Eddy Numerical Simulations of Turbulent Flows," AIAA Journal, Vol. 15, Sept. 1977, pp. 1261-1267.

15 Hama, F. R., "Progressive Deformation of a Curved Vortex Filament by its Own Induction," Physics of Fluids, Vol. 5, No. 10, Oct. 1962, pp. 1156-1162.

16 Deardorff, J. W., "A Numerical Study of Three-Dimensional Turbulent Channel Flow at Large Reynolds Number," Journal of Fluid Mechanics, Vol. 41, Part 2, April 1970, pp. 453-480.

17 Schumann, U., "Subgrid Scale Model for Finite Difference Simulations of Turbulent Flows in Plane Channels and Annuli," Journal of Computational Physics, Vol. 18, No. 4, Aug. 1975, pp. 376-404.

18 Moin, P., Reynolds, W. C., and Ferziger, J. H., "Large Eddy Simulation of Incompressible Turbulent Channel Flow," TF-12, May 1978, Dept. of Mechanical Engineering, Stanford Univ., Stanford California.

19 Orszag, S. A. and Kells, L. C., "Transition to Turbulence in Plane Poiseuille and Plane Couette Flow," Cambridge Hydrodynamics Rept. 10, May 1978.

20 Wray, A. A., Hussaini, M. Y., and Degani, D., "Numerical Simulation of Transition to Turbulence," Proceedings of the Second Gamm Conference on Numerical Methods in Fluid Mechanics, DFVLR, Köln, West Germany, 1977, pp. 247-254.

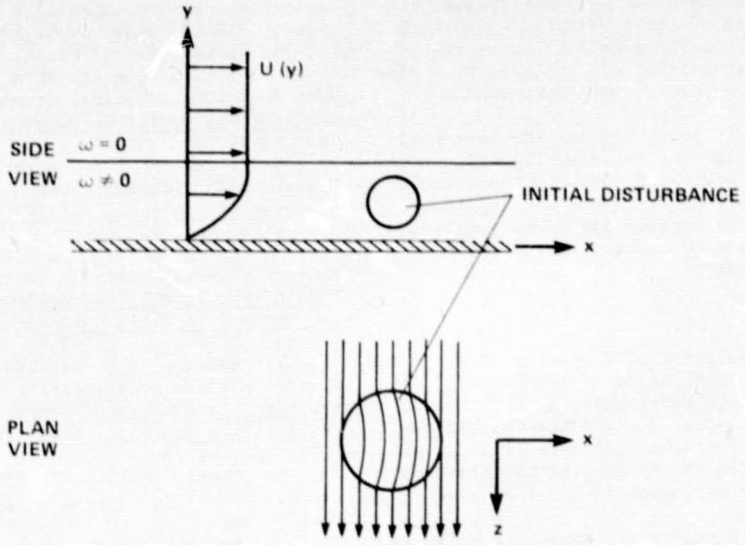

Figure 1.- Spot geometry.

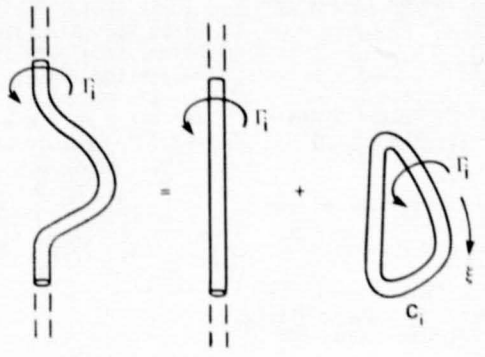

Figure 2.- Decomposition of vorticity field.

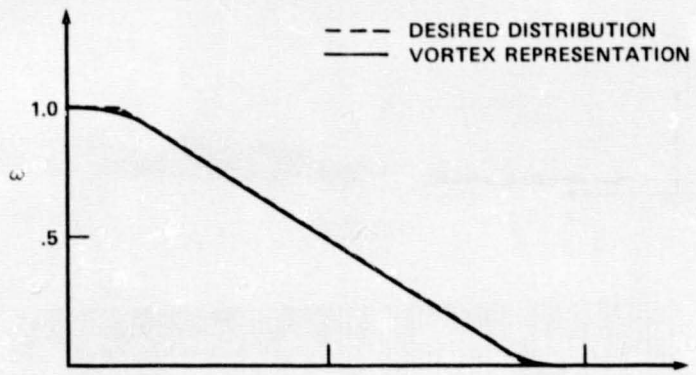

(a) Optimum vortex representation.

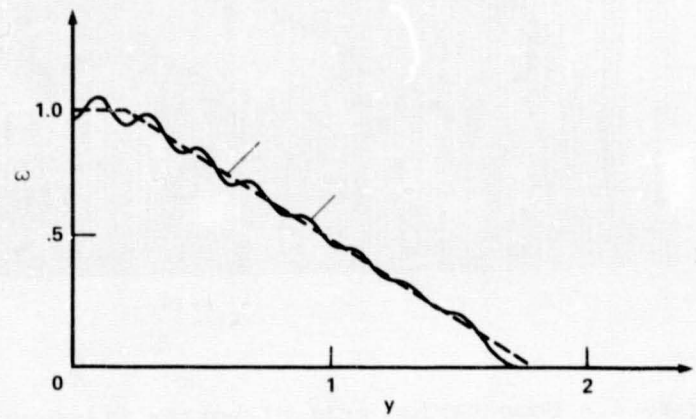

(b) Suboptimum choice of core size.

Figure 3.- Vorticity distributions.

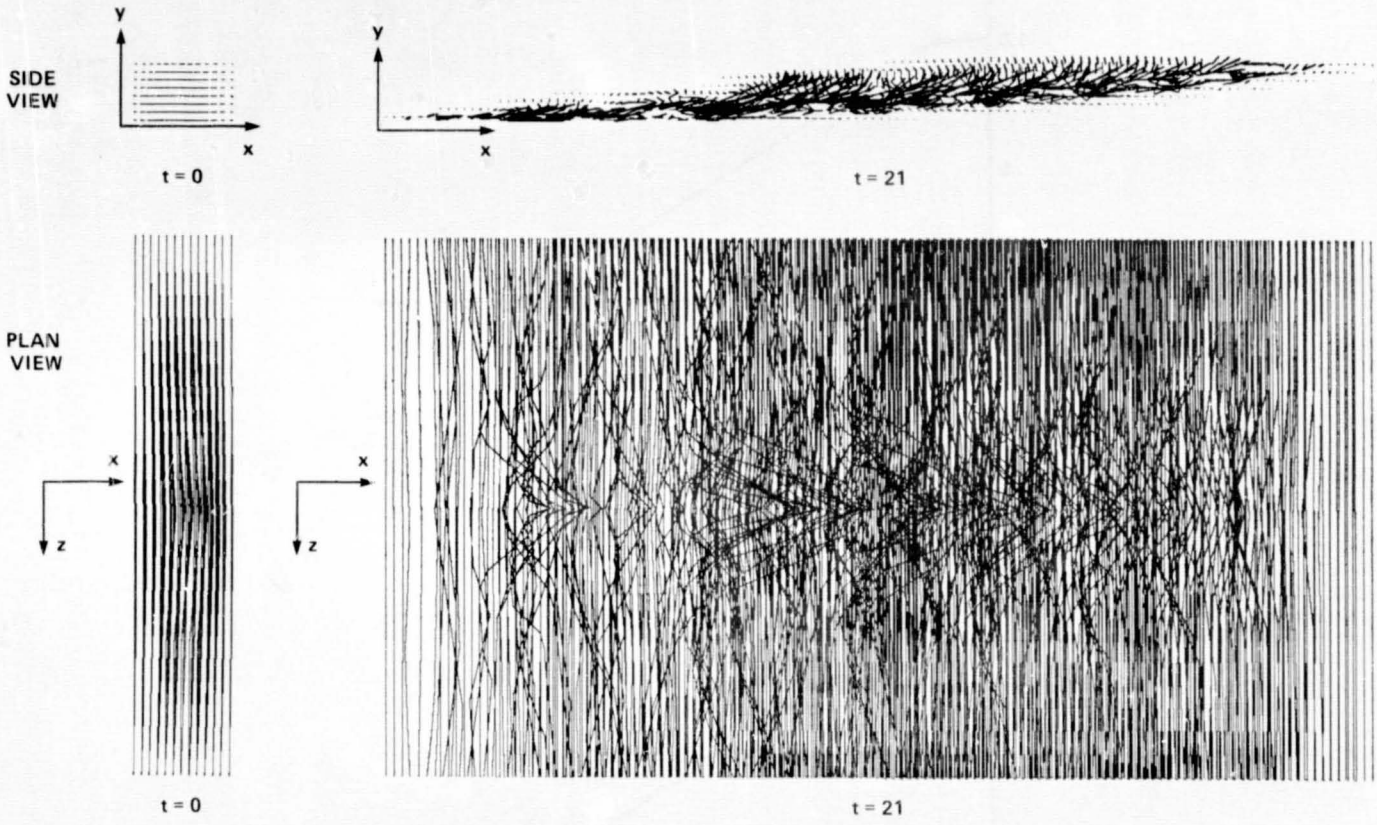

Figure 4.- Computation grid of vortex filaments.

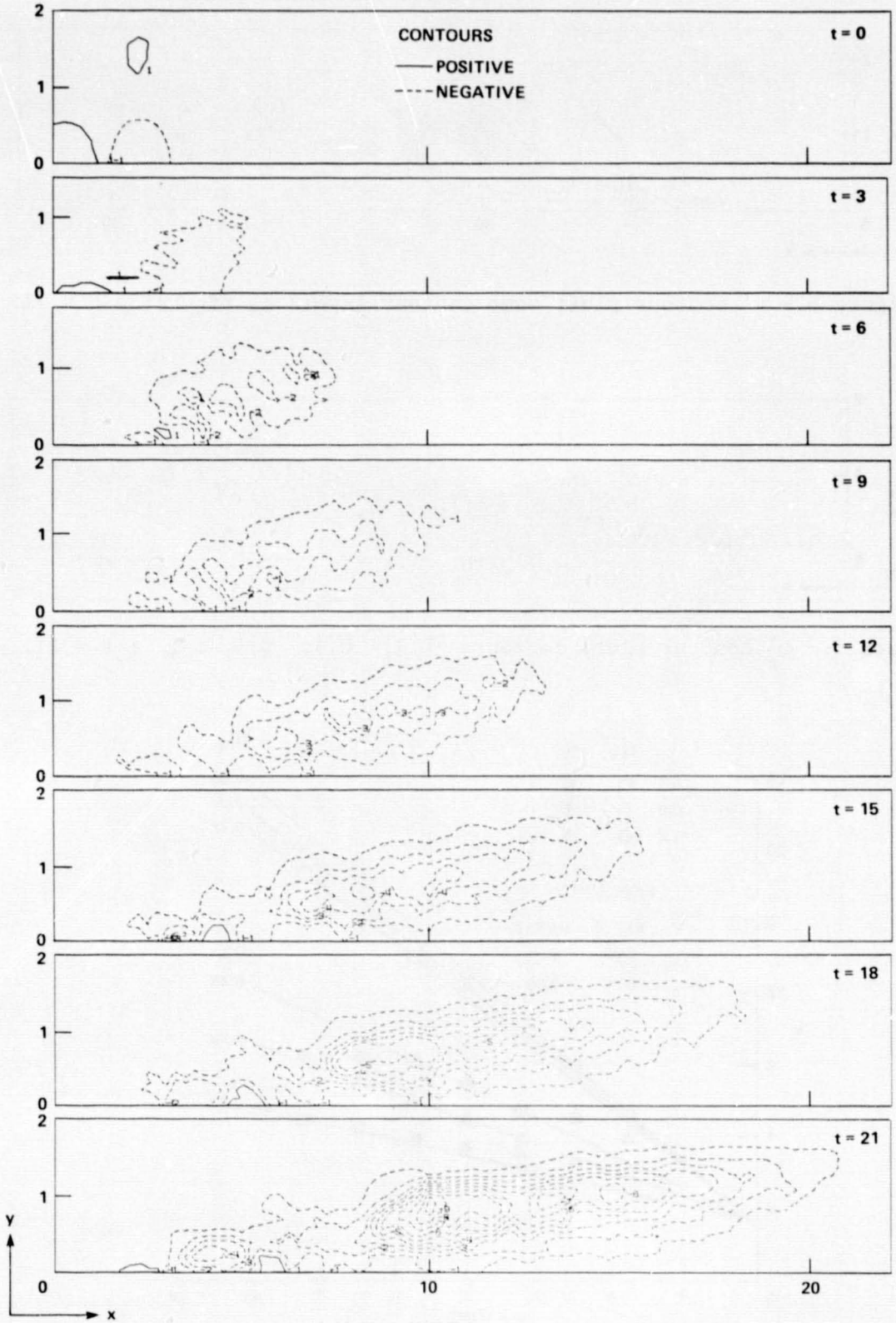

Figure 5.- u' contour plots, y scale expanded by 2; contours ±0.02, ±0.06, ±0.10, . . .

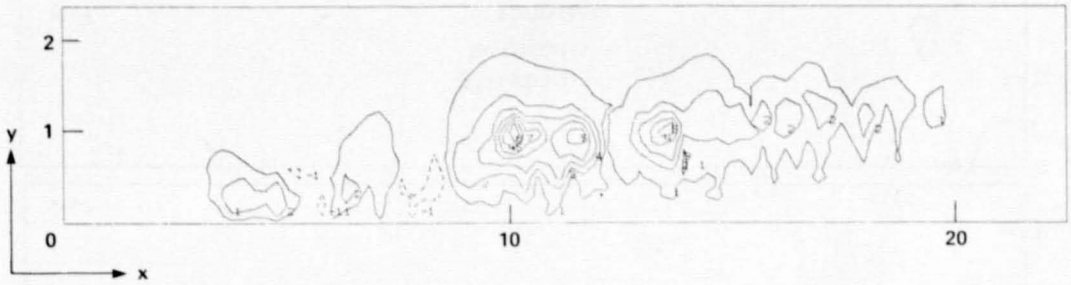

Figure 6.- v' contour plot; same contour levels as figure 5; t = 21.

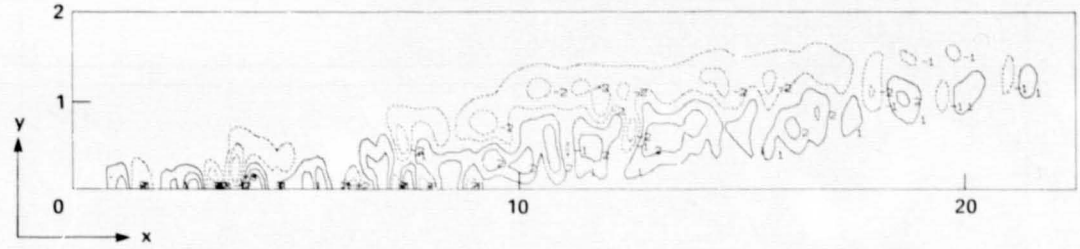

Figure 7.- ω_z' contour plot; contours 0.1, 0.3, 0.5, . . .; t = 21.

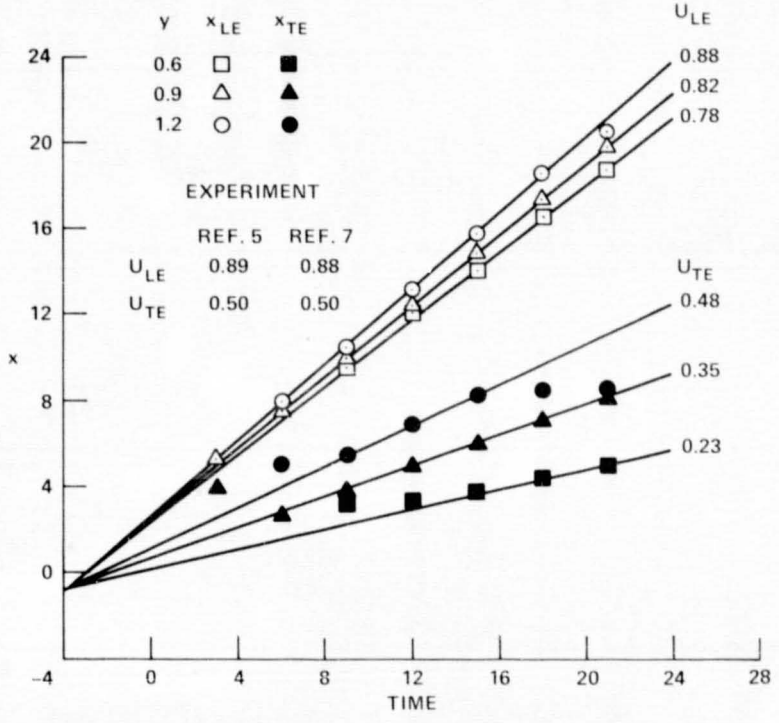

Figure 8.- Trajectories of leading and trailing edges.

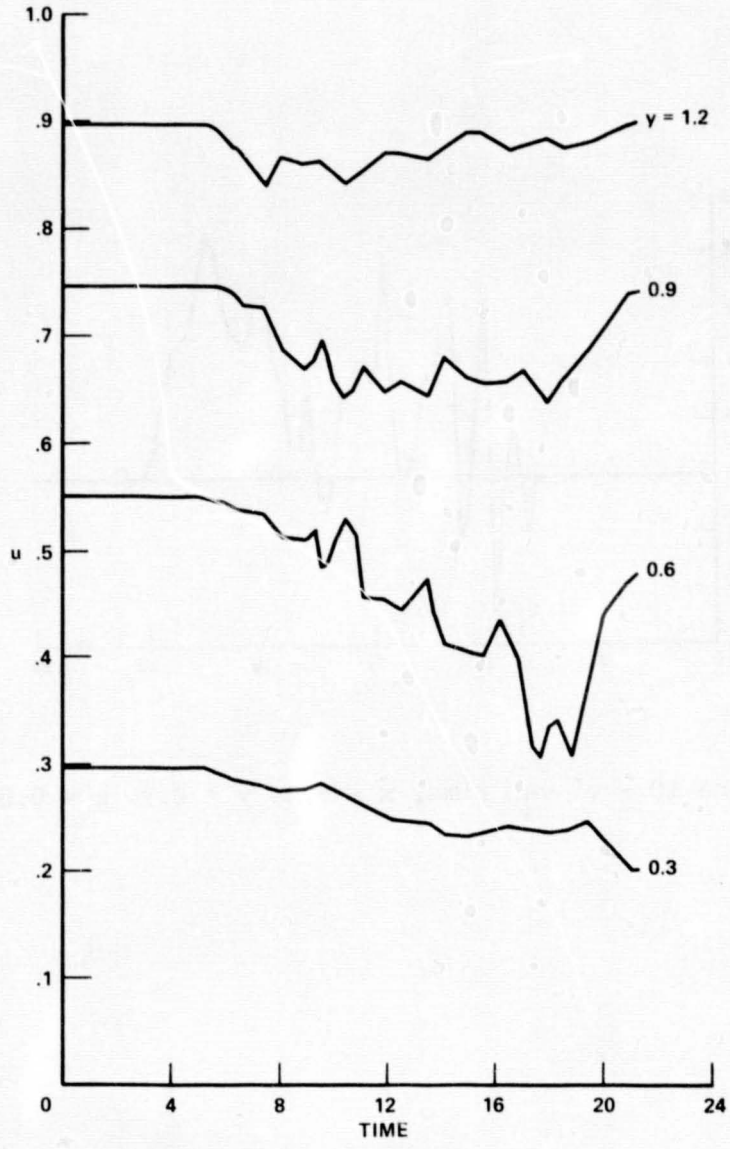

Figure 9.- u vs time, x = 8.0, z = 0.0.

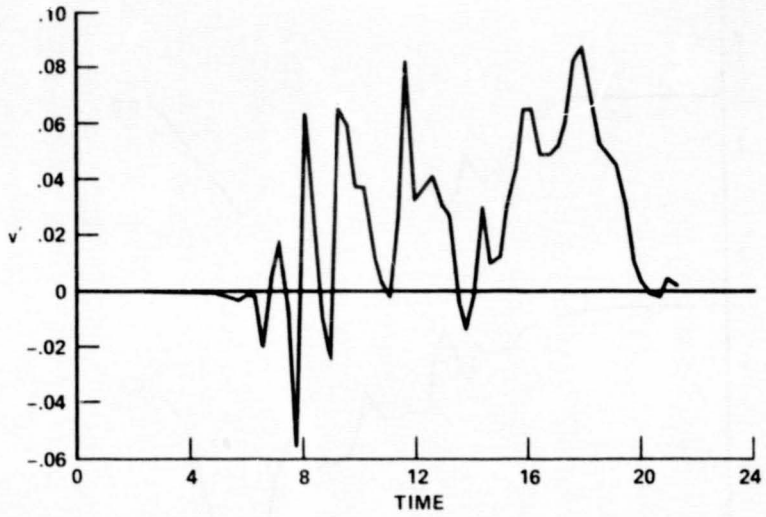

Figure 10.- v' vs time, x = 8.0, y = 0.9, z = 0.0.

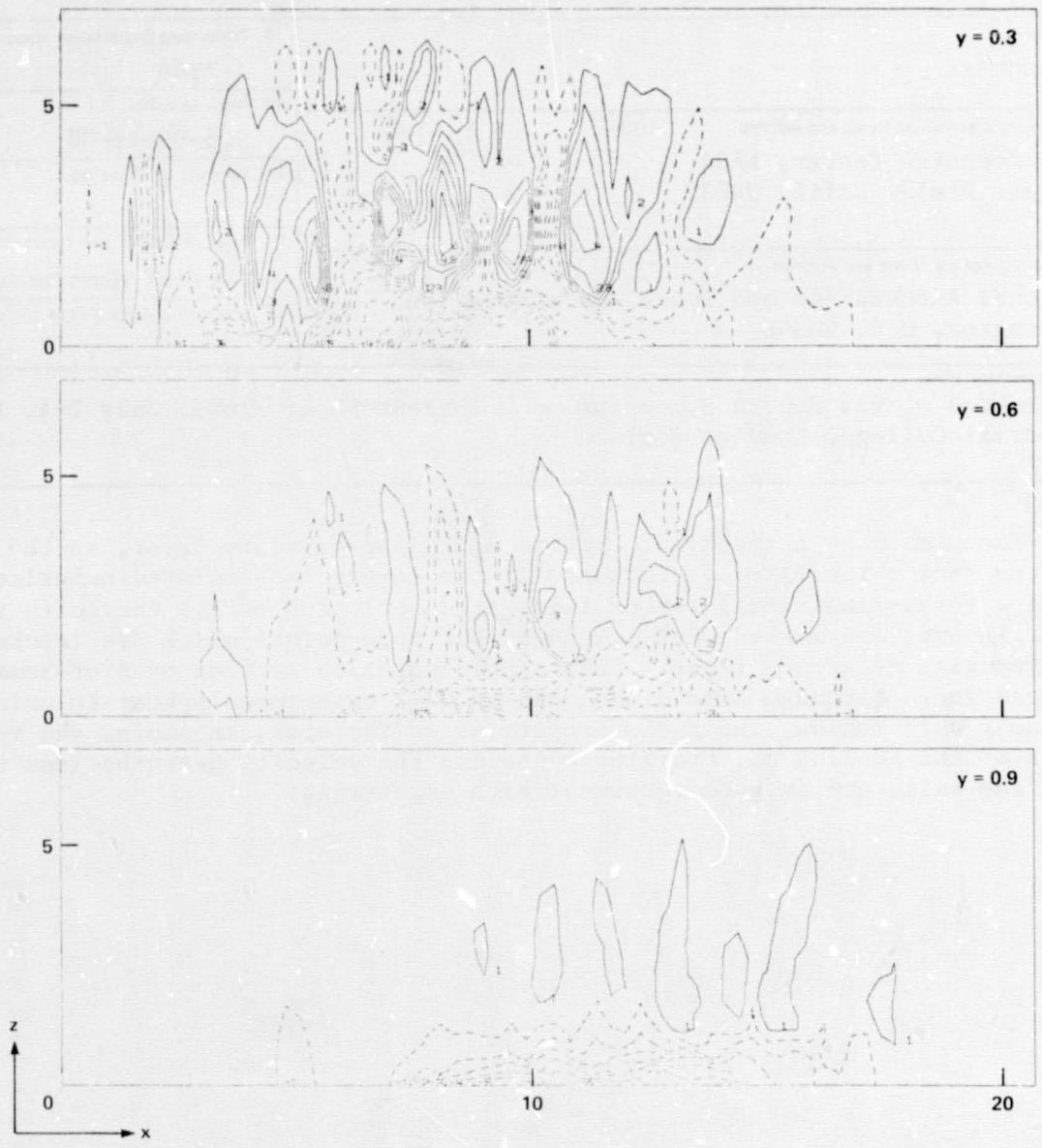

Figure 11.- u' contour plots in horizontal planes;
contour levels ±2%, ±6%, ±10%, . . .